Contact angles and wetting behaviour of single micron-sized particles

2005 J. Phys.: Condens. Matter 17 S445

(http://iopscience.iop.org/0953-8984/17/9/011)

INSTITUTE OF PHYSICS PUBLISHING JOURNAL OF PHYSICS: CONDENSED MATTER

J. Phys.: Condens. Matter **17** (2005) S445–S464 doi:10.1088/0953-8984/17/9/011

Contact angles and wetting behaviour of single micron-sized particles

Graeme Gillies, Karsten Büscher, Markus Preuss, Michael Kappl, Hans-Jürgen Butt and Karlheinz Graf

Max Planck Institute for Polymer Research, Ackermannweg 10, D-55128 Mainz, Germany

E-mail: grafk@mpip-mainz.mpg.de

Received 24 November 2004
Published 18 February 2005
Online at stacks.iop.org/JPhysCM/17/S445

Abstract

A 'particle interaction apparatus' based on the technique of atomic force microscopy was constructed that allows us to measure the interaction between single micron-sized particles and the air–water interface. From the force versus distance profiles ('force curves') the contact angle of single microspheres could be determined. This new method for microsphere tensiometry was validated using a variety of materials with contact angles between 20° and 90°. Contact angles measured on single microspheres correlated well with those measured on flat substrates of the same materials.

The interaction of single silica microspheres with an air bubble in the presence of surfactants (SDS and DTAB) was investigated. Depending on surfactant type and concentration, adhesion or repulsion could be induced. Adhesion forces were found to depend on the applied load, indicating possible adsorption/desorption processes at the particle–bubble interface.

We have built a new set-up that combines a particle interaction apparatus with a Langmuir trough and a fluorescence microscope. This will allow study of interactions at the air–water interface in more detail, especially in the presence of a definite surface density of amphiphilic molecules.

The interaction of single ZnS spheres with a bubble (modelling flotation of ZnS) was studied at different pH values. The results suggest that the isoelectric point of these spheres exists between pH 7 and 8.

(Some figures in this article are in colour only in the electronic version)

1. Introduction

1.1. Microsphere tensiometry

The wetting behaviour of small particles is important in many industrial applications and natural phenomena. Examples are the pigment, paint, cosmetic, pharmaceutical and food

industries, that all require knowledge of particle wettability for product design and production processes. The wettability is usually characterized in terms of the solid–liquid contact angle. For particles, this important parameter is usually measured with the capillary rise method [1–5]. In a capillary rise experiment a tube, which is closed by a filter at the bottom, is filled with the particles in the form of a powder. The bottom of the tube is brought into contact with the liquid. The liquid rises in the tube due to the capillary effect of the voids between the powder particles. From the rising speed or the pressure needed to stop the rise of the liquid the contact angle can be calculated, assuming that the powder behaves like a bundle of capillaries [6–8]. One limitation of the capillary rise method is that it averages over many particles. In addition, it relies on the assumption that a powder can be treated as a bundle of capillaries and depends on the specific model applied [9].

The interaction between air bubbles and colloidal particles is of special interest for applications like flotation, water purification, and the deinking of paper. In flotation mineral particles are selectively separated on the basis of their different capture rates by air bubbles [10, 11]. Since most of the world's minerals are separated by flotation, much attention has focused on understanding and controlling the interactions between particles and bubbles. When modelling flotation on the basis of its elementary processes the flotation efficiency P_{Flot} can be written as the product of three factors [11]: $P_{\mathrm{Flot}} = P_{\mathrm{Coll}} \cdot P_{\mathrm{Attach}} \cdot P_{\mathrm{Det}}$. P_{Coll} is the hydrodynamic capture probability, which describes the probability for collision between particles and bubbles. P_{Attach} is the probability that particles colliding with a bubble rupture the water film, attach to the bubble by forming a three-phase contact line. P_{Det} is the probability that a particle attached to a bubble does not detach again.

The probability that a captured particle does not detach from a bubble again is determined by its contact angle. Actual detachment forces of air bubbles from sulfur and graphite rods of 0.1 mm diameter were in the range 100 μN [12].

Contact angles of nanometre-sized particles have been deduced by spreading particles on a liquid surface in a Langmuir trough [13, 14]. From the surface pressure–area relationship the contact angle could be calculated. This technique again gives an average contact angle of many particles. A quantitative method to measure the contact angle of large particles is sphere tensiometry. Originally sphere tensiometry was used to measure the surface tension of a liquid [15–18]. Therefore the force required to pull a sphere out of a liquid is measured. From this force the surface tension of the liquid can be calculated. Later, contact angles were also determined by measuring whole force-versus-pull-out-distance curves [19–22]. For sphere tensiometry typically particles with diameters of several hundred micrometres are used.

The forces between colloidal particles of 2–20 μm diameter and air bubbles were also measured directly [23–26] using the so-called colloidal probe technique. In such direct force-versus-separation measurements a single particle is fixed to the end of an AFM cantilever that is acting as a force sensor (figure 1). The particle is moved in aqueous medium towards an air bubble by means of a piezoelectric actuator. To measure the deflection of the cantilever and thus the force, a laser is reflected from the backside of the cantilever onto an optical detector (usually a split photodiode). Multiplying the measured cantilever deflection with the spring constant of the cantilever gives the force. In this way force versus position can be recorded and converted to force-versus-separation curves. This experimental technique can also be exploited for microsphere tensiometry that allows the determination of contact angles for single micron-sized particles. From force-versus-position measurements between spherical particles and bubbles the contact angle can be calculated. Figure 2 (upper part) shows a schematic diagram of a typical force versus position signal obtained in such a microsphere tensiometry experiment with a particle having a contact angle significantly larger than zero. At large separations between bubble and particle, no force is acting and the cantilever deflection

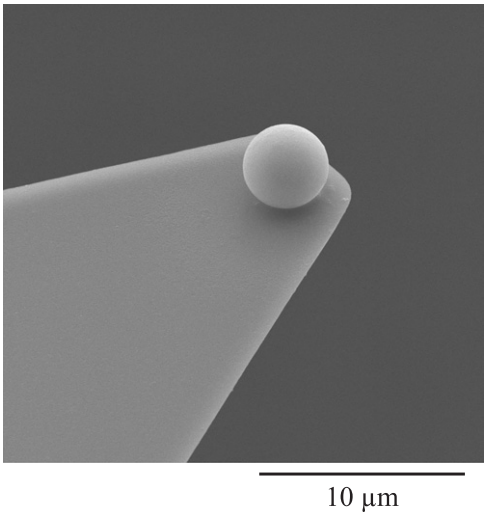

Figure 1. Silanized silica sphere glued to the end of an AFM cantilever to act as a colloidal probe.

results in the zero-force line (a). When the particle and bubble get into contact (b), a jump-in occurs and a three-phase contact line is formed (c). During further approach of the bubble, one reaches a point where no force is acting on the particle (d). This is where the force curve crosses the zero-force line. At this equilibrium position the particle with radius R has moved a distance D into the air bubble (lower part of figure 2). From this distance the contact angle can be calculated [27, 28]

$$\cos \Theta_{\mathrm{r}}^{\mathrm{sphere}} = \frac{R - D}{R}. \tag{1}$$

In the approaching part of the force curve the three-phase contact line (TPL) is receding, since less and less of the particle surface is covered by the liquid. Therefore we denote it the 'receding contact angle' $\Theta_{\mathrm{r}}^{\mathrm{sphere}}$. Further movement of the particle against the bubble leads to an increased deflection of the cantilever (e). When the movement is reversed, an adhesion of the particle to the bubble will be observed for hydrophobic particles, leading to an negative deflection of the cantilever (f). When the restoring force of the cantilever becomes larger than the adhesion force, the particle will snap out of the bubble (g).

In our group we have developed an instrument called a 'particle interaction apparatus' (PIA) (figure 3), that is based on the measurement principle of standard AFMs but has some advantages over commercial ones [26]. The piezoacutator for controlling the distance between bubble and colloidal probe has a relatively large operating range of 12 μm that allows detachment of the particle from the bubble after contact. An integrated capacitive distance sensor allows the operation of the piezoactuator in a closed loop mode where the position of the bubble can be controlled with nanometre precision. A position sensitive device with an active area of 20×20 mm^2 detects the deflection of the reflected laser beam. This results in a larger detection range for the measured interaction forces.

Figure 4 shows the comparison of contact angles measured for single spheres by microsphere tensiometry with contact angles measured for flat substrates using the sessile drop method [29]. The spheres used for these experiments are either polystyrene spheres with radii of 1.8 and 4.4 μm or silica spheres of 2.0–2.4 μm that were coated in one of the following ways to adjust the contact angle: (1) silanation with dichlorodimethylsilane (DMDS),

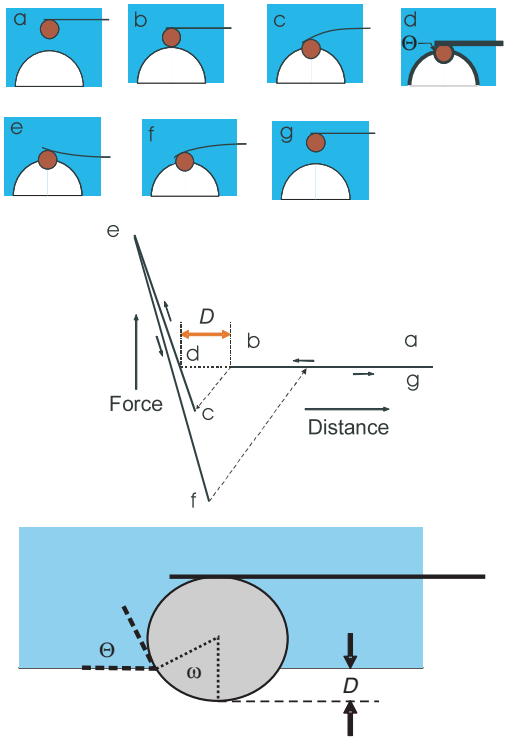

Figure 2. Upper part: schematic diagram of a force versus distance curve for a hydrophobic colloidal probe contacting a bubble in aqueous solution. (a) Far from the bubble surface, no deflection of the AFM cantilever is observed (= zero-force line). (b) When the sphere gets in contact with the bubble, a snap-in occurs and (c) a three-phase contact line is formed. When approaching further, the force curve crosses the zero-force line (d). At this point the particle has moved the distance D into the bubble. Lower part: relation between jump-in distance D, immersion angle ω and contact angle Θ.

(2) silanization with hexadimethylsilazane (HDMS) or (3) gold coating by sputtering plus a monolayer of alkylthiols (mixtures of hydroxyl terminated undecanethiol and undecanethiol at different molar fractions) [30–32]. Mixtures with a high mole fraction of hydroxy alkylthiols led to small contact angles. With increasing mole fraction of pure alkylthiols the contact angle increased [33]. The results presented in figure 4 confirm that the contact angles with water for microspheres of different sizes, chemical compositions, and hydrophobicities are well correlated with the contact angles on planar substrates prepared in a similar way. For contact angles above roughly 40° the values for microspheres and planar surfaces were in good agreement. Below roughly 40°, we observed higher contact angles on the microspheres than on the planar substrates. A possible reason could be a negative line tension. For contact angles below 90° a negative line tension would lead to a deviation of the apparent contact angle Θ (as determined by microsphere tensiometry) from the 'real' contact angle ϑ (as determined on a planar substrate without the influence of the three-phase contact line), that is given by [34]

$$\sin\varepsilon = \frac{\kappa}{R\gamma}\frac{\cos\Theta}{\sin^2\Theta} \tag{2}$$

where $\varepsilon = \Theta - \vartheta$, R is the radius of the sphere, γ is the surface tension of the liquid and κ is the line tension. With typical values ($\vartheta = 30°$, $\Theta = 38°$) we estimate $\kappa = -10$ nN.

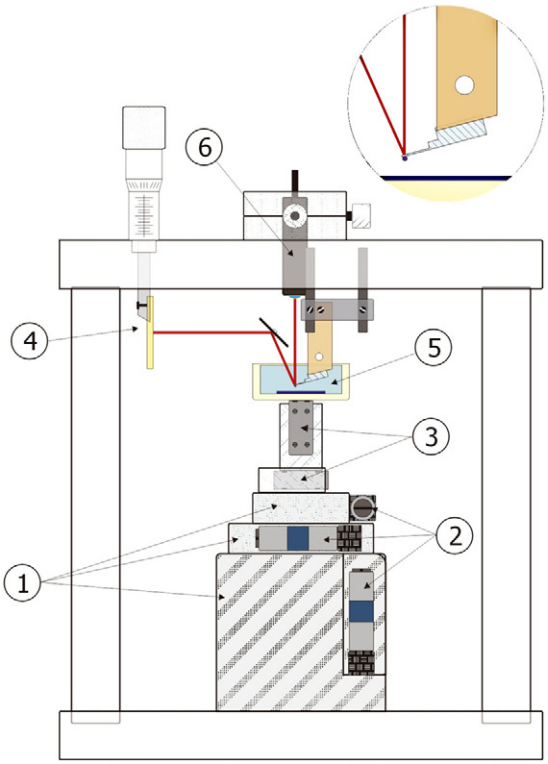

Figure 3. Schematic diagram of the particle interaction apparatus (PIA): (1) x–y–z translation stage, (2) stepper motors for controlling the x–y–z stage, (3) piezos for horizontal and vertical displacement, (4) PSD for monitoring the cantilever deflection, (5) liquid cell with substrate on the bottom, cantilever with glued particle fixed on a holder from above, (6) 670 nm laser light source, movable in the x–y direction to focus it on the backside of the cantilever.

Values of one order of magnitude larger have been found for polystyrene particles ($\Theta = 90°$) by determination from the size dependence of the apparent contact angle [34]. This, however, is not surprising since the materials and degree of hydrophobicity were different in the two cases. For the case of the polystyrene spheres, contact angles of microspheres showed a good agreement with the value on a flat substrate but large variations were observed. This may be attributed to the higher surface roughness of the polystyrene particles compared to silica particles. The increased roughness is expected to lead to increased pinning of the TPL and contact angle hysteresis and therefore to larger variations in the measured contact angles.

1.2. Influence of surfactants on particle bubble interaction

Surfactants are widely used in flotation to modulate particle bubble interaction in order to improve the efficiency of the flotation process. The colloidal probe technique is an excellent tool to directly investigate the influence of surfactants on particle bubble interaction. We have studied the influence of the surfactants sodium dodecyl sulfate (SDS) and dodecyltrimethylammonium bromide (DTAB) on the interaction between silica spheres and an air bubble [26]. DTAB adsorbs strongly to silica and is positively charged. SDS does not adsorb to silica and is negatively charged. The properties of both substances are well studied. Their critical micelle concentrations (cmcs) are 16 mM for DTAB and 8 mM for SDS [35].

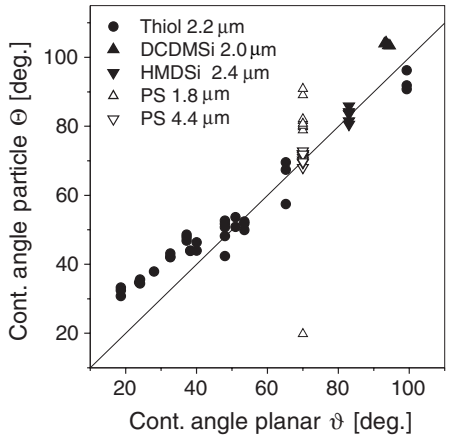

Figure 4. Contact angles for microspheres in water plotted versus the receding contact angles measured on similarly prepared planar surfaces. (●) Silica microspheres with a radius of 2.2 μm which were coated with gold and a self-assembled thiol monolayer of undecanethiol and hydroxy-terminated undecanethiol. Contact angles were adjusted by varying the molar ration of the two components [33]. (▲) Silica microspheres of 2 μm radius treated with dichlorodimethylsilane [59]. (▼) Silica microspheres of 2.4 μm radius treated with hexamethyldisilazane [34]. (△) Polystyrene microspheres with radii of 1.8 μm and (▽) 4.4 μm [34].

Hydrophobic particles with SDS. Silica particles of 5 μm diameter were hydrophobized by exposing them to an atmosphere of dichlorodimethylsilane for a few minutes. When approaching an air bubble with these particles, a jump-in occurred (figure 5, upper). We assigned separation zero to this position. A TPL was established and the capillary force dominated. In some cases a small repulsive force of typically $F/R \approx 10^{-4}$ N m^{-1} was observed before contact. The repulsive force decayed exponentially with a decay length similar to the Debye length. Hence, it is probably mainly the electrostatic double-layer force. Since silanized silica particles bear a negative surface charge [36] they are repelled by the negatively charged bubble. Once a TPL was established, the force curve increased steeply. During the approach the force curve was slightly bent and not perfectly linear. When the particle was retracted again, the force curve became even steeper and the force decreased in a purely linear way. Hence, we believe that during approach the TPL was moving; when retracting again it was pinned. A relatively large normalized force of about 70 mN m^{-1} was necessary to pull the particle out of the bubble again. In flotation this adhesion force would prevent the particle from detaching from the bubble. When small amounts of SDS were added, the repulsion increased (figure 5, middle). However, with increasing SDS concentration not only was the exponentially decaying force component observed but in addition a high force component increased linearly (figure 5, lower). At closer distances a jump-in was usually observed and a TPL was formed if the loading force exceeded a certain threshold value (figure 6). If a jump-in occurred and a TPL was formed, strong adhesion was observed and the particle had to be pulled out off the bubble again with a high force. Above the threshold the adhesion was almost constant and no longer significantly depended on the load, which is the maximal force with which the particle was pushed against the bubble. If the load did not exceed the threshold, the approaching and retracting parts of the force curve were reversible and no adhesion was observed. The threshold force increased with increasing SDS concentration (figure 7). Above a concentration of roughly 6 mM SDS, no jump-in and only repulsive forces were observed.

The reason for the increase of the repulsion with increasing SDS concentration is probably that SDS adsorbs to the hydrophobic silica surface and to the air–water interface. Hence, one

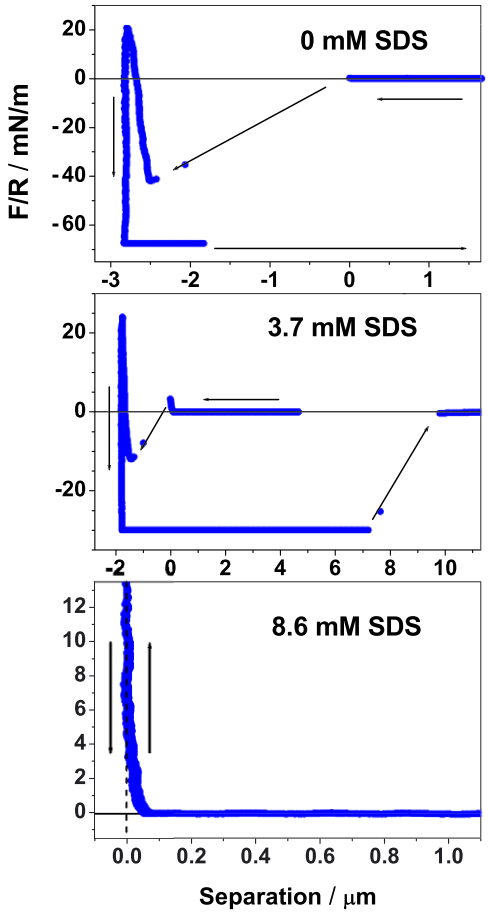

Figure 5. Normalized force (F/R) versus separation curves measured with a hydrophobic silica particle in aqueous electrolyte solutions without SDS, with 3.7 mM SDS and with 8.6 mM SDS plus 0.3 mM KCl. Please note that the scales are different.

would expect an increase of the electrostatic force with increasing SDS concentration up to the cmc. This hypothesis is supported by results of Dai *et al* who measured the attachment of argon bubbles to mercury at different SDS concentrations [37]. They observed an initial repulsion, which increased with increasing SDS concentrations.

Hydrophobic particle with DTAB. The behaviour was similar to the results observed when adding SDS: with increasing DTAB concentration the repulsion increased, the jump-in distance decreased, and the adhesion also decreased (figure 8). As before the threshold behaviour of the adhesion on load was observed and the threshold load increased with increasing DTAB concentration (figures 6 and 7). Hence, the behaviour is qualitatively the same as with SDS; it is only shifted to higher surfactant concentrations. This, however, is expected since the cmc of DTAB is higher than that of SDS.

Hydrophilic particles in aqueous electrolyte containing DTAB. Without DTAB only repulsion could be observed (figure 9). At concentrations between 0.1 mM and typically 5 mM, no

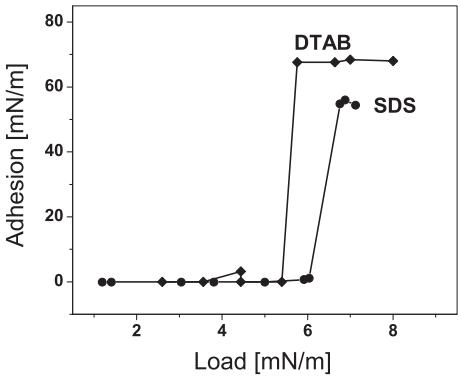

Figure 6. Normalized adhesion force versus load for hydrophobic particles in 5.6 mM SDS (●) and 11.4 mM DTAB (♦) plus 0.3 mM KCl. Above a concentration of 6 mM (SDS) or 12 mM (DTAB) no jump into three-phase contact was observed any longer. Adhesion force is the force necessary to pull the particle out off the bubble, load the maximal force with which the particle is pushed against the bubble.

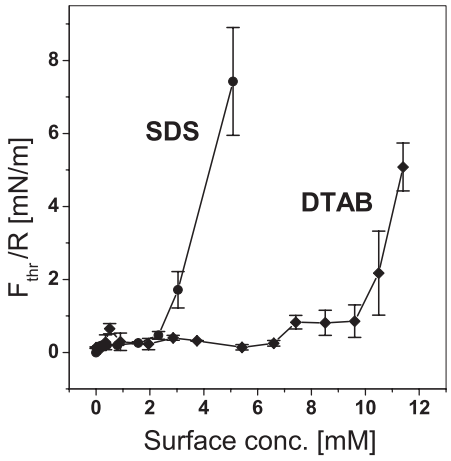

Figure 7. Normalized threshold force (F_{thr}/R) necessary to overcome the repulsion barrier versus SDS (●) and DTAB (♦) concentration for a hydrophobic particle in 0.3 mM KCl. Above a concentration of 6 mM (SDS) or 12 mM (DTAB) no jump into three-phase contact was observed any longer.

repulsion and only strong attraction was observed which led to a jump-in and TPL formation. The resulting contact angle increased from 35° at 0.1 mM DTAB to 50° at 5.4 mM DTAB (figure 10). The adhesion slightly increased from 380 nN, equivalent to a normalized force of 0.15 N m^{-1}, to 430 nN, equivalent to 0.17 N m^{-1}. After the jump into contact, we again observed that the slope of the force versus position curve was steeper (and strictly linear) on the retracting part than during advance. Hence, the TPL was probably moving during the advance and it was pinned when retracting the particle. These results can be explained with the strong adhesion of DTAB to silica and with the gradual lowering of the surface tension of water up to the cmc. DTAB forms a monolayer on silica even at concentration as low as 0.1 mM [38]. Its adsorption to silica has two effects. First, it renders the silica surface hydrophobic. This results in a hydrophobic attraction. Second, DTAB reverses the surface charge to positive and the electrostatic force between the negatively charged bubble surface and the positively charged particle becomes attractive. The increase of the contact angle from 0° of bare silica to 35° measured at 0.1 mM demonstrates the hydrophobizing effect of DTAB. The further increase from 34° to 50° at 5.4 mM DTAB can probably be attributed to the lowering of the surface tension of water. This agrees with results of Eriksson *et al* obtained with hexadecyltrimethylammoniumbromide (CTAB) [39]. They showed that the contact angle of an aqueous CTAB solution on mica increases with increasing CTAB concentration up to a maximum around 0.03 mM (contact angle $\approx$ 72°) then it decreases again. The strong adsorption of DTAB to silica and the decrease of the surface tension of water could also explain the relatively small change in adhesion.

When the DTAB concentration was increased to 5.4 mM, a small electrostatic repulsion was observed before the jump-in. Above roughly 6 mM DTAB the jump-in disappeared and a repulsive component occurred and completely dominated. This transition around 6 mM DTAB between a pure jump-in and the repulsion was usually a discrete change. Only in some cases a repulsive force was observed at lower concentrations before the jump-in. The repulsion

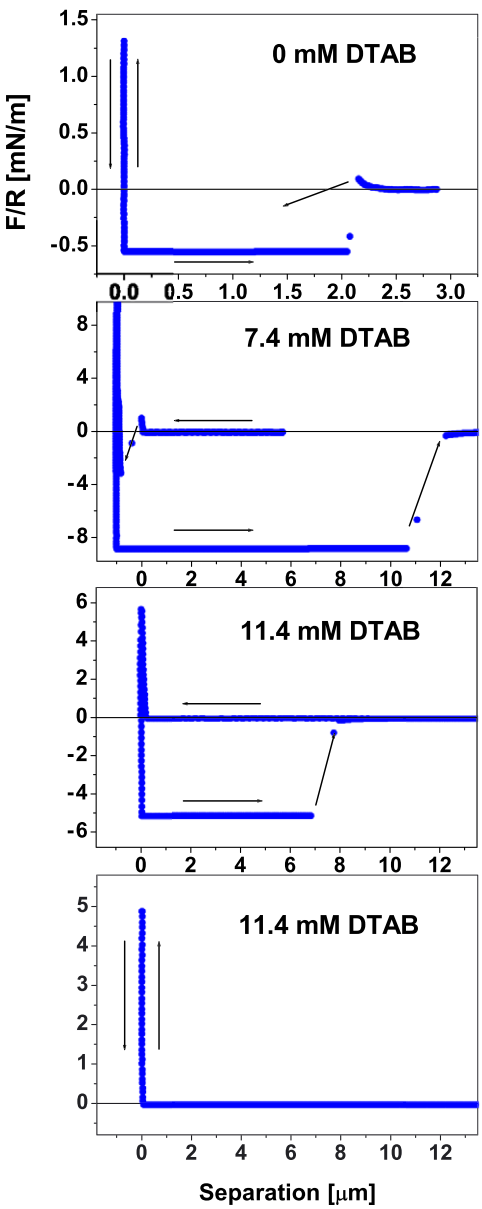

Figure 8. Normalized force (F/R) versus separation measured with a hydrophobic silica particle in aqueous electrolyte (0.3 mM KCl) with no added DTAB, 7.4 mM DTAB, and twice 11.4 mM DTAB. The first curve at 11.4 mM DTAB was obtained when the load exceeded the threshold force. In the second case the load remained below the threshold force of roughly 0.005 N m^{-1}. Please note that the scales are different.

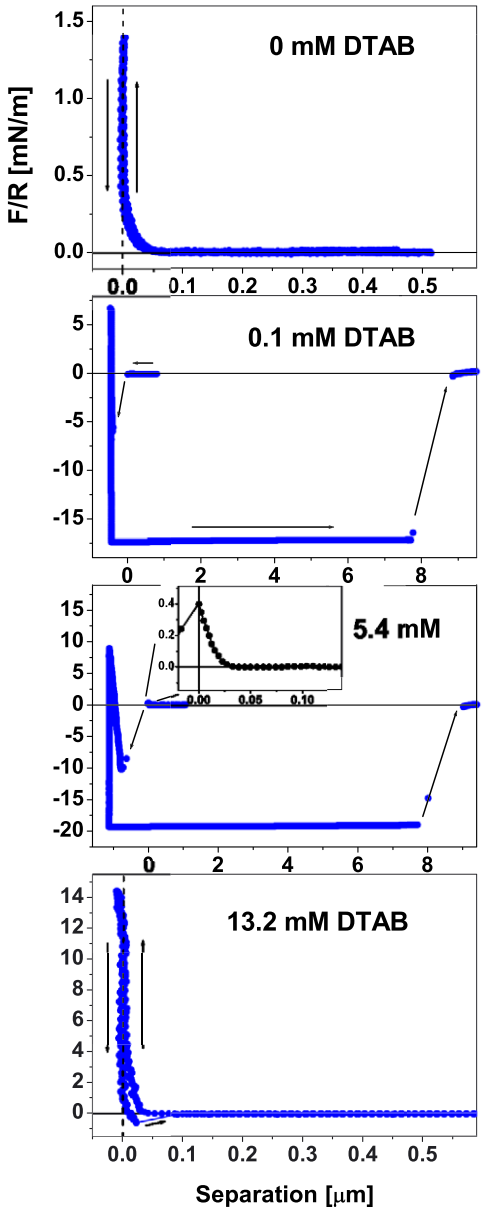

Figure 9. Normalized force (F/R) versus separation curve measured with a hydrophilic silica particle in aqueous electrolyte with no added DTAB, 0.1 mM DTAB, 5.4 mM DTAB, and 13.2 mM DTAB. The inset at 5.4 mM shows the electrostatic repulsion before the jump-in.

was at least partly due to electrostatic repulsion since it decayed exponentially with the Debye length. The reason is probably that at DTAB concentrations above 5 mM the air–water interface

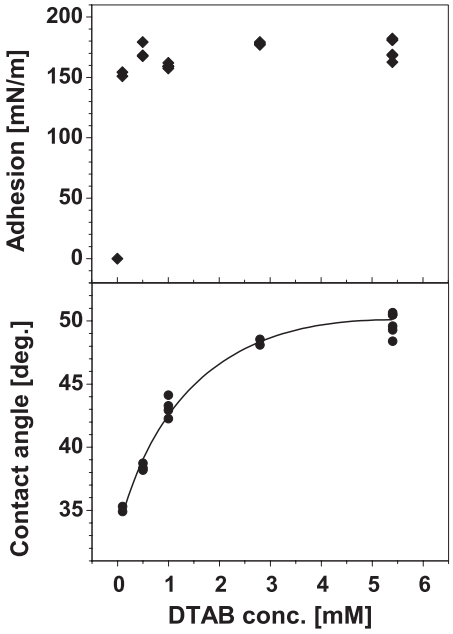

Figure 10. Normalized adhesion (force necessary to pull the particle off the bubble divided by its radius) and receding contact angle for a hydrophilic particle in 0.3 mM KCl at various DTAB concentrations. The contact angles were determined from measuring the jump-in distance D. No jumps into three-phase contact were observed above concentrations of roughly 6 mM DTAB.

also becomes positively charged due to adsorbed DTAB leading to an electrostatic repulsion. This electrostatic repulsion is, however, probably not the only repulsive force because beyond the exponential increase the force was still repulsive and a stable water film was formed on the particle surface. Probably other forces such as the hydration force kept the water film stable. The force curves at DTAB concentration above 6 mM were not reversible. When retracting the particle an adhesion was observed. The adhesion increased monotonically with the applied load (figure 11). This is in marked contrast with the behaviour observed at low DTAB concentrations. At low concentrations the adhesion was constant and did not depend on the load. It is also completely different from the threshold behaviour observed with SDS and DTAB on hydrophobic particles. In both cases the adhesion was independent of the applied load. We have as yet no explanation for the monotonic increase of the adhesion versus load. It might be due to a change of the surfactant structure at the interfaces when the particle comes close to the air–water interface. With increasing DTAB concentration the adhesion had a tendency to decrease (figure 11). The reason is probably the decrease in the surface tension of water.

2. Particle bubble interaction for spherical ZnS particles

2.1. Experimental details

2.1.1. Materials. Analytical grade $Zn(NO_3)_2$, KNO_3, ethanol, dichlorodimethylsilane and thioacetamide were obtained from Sigma-Aldrich Chemie (Steinheim, Germany). Deionized water was further purified with a Milli-Q water purification system consisting of ion exchange, activated carbon stages and final filtration through a 0.22 μm filter. The water possessed a final resistivity of 18.2 MΩ cm.

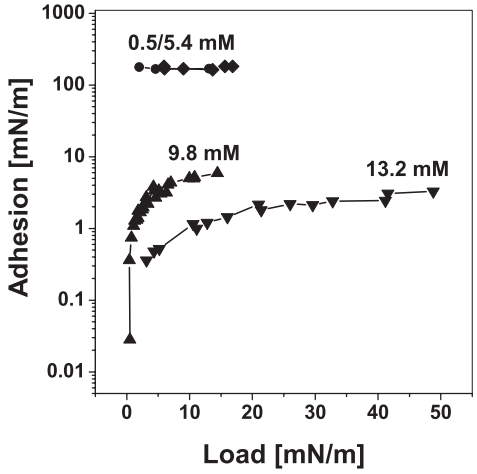

Figure 11. Adhesion versus load for hydrophilic silica particles at different DTAB concentrations as indicated.

2.1.2. Sample cleaning. All glassware and relevant surfaces were cleaned immediately prior to use with saturated KOH solution followed by extensive rinsing with Milli-Q water. Such a process is likely to roughen silica surfaces, thus silica colloid probes and silica surfaces were only subject to KOH solutions for a minimal duration. Cantilevers with mounted ZnS particles did not undergo such treatment and were instead rinsed in analytical grade ethanol filtered through a 0.22 μm membrane filter.

2.1.3. Sample substrates. Silica substrates were fashioned from polished silicon plates which possessed an outer layer of silica (500 nm) formed by roasting in a diffusion oven. For particle–bubble interactions, silica substrates had to be first modified by exposing clean silica surfaces to dichlorodimethylsilane vapour for 2 min. Bubbles (typically 200 μm in diameter) could then be attached to immersed silanated surfaces by pressing an air bubble formed on the end of a syringe against the surface.

2.1.4. Particles. Monodisperse borosilicate particles, diameter 5.1 ± 0.5 μm, were supplied by Duke Scientific Corporation (Palo Alto, USA) and were assumed to behave as silica particles.

Zinc sulfide spheres were synthesized using a modified version of the method reported by Wilhelmy and Matijevic [40]. First 5.7 g of thioacetamide was dissolved in 200 ml of water, via brief sonication. 50 ml of 0.06 M $Zn(NO_3)_2$ solution was added and the reaction vessel was sealed and left at room temperature for four hours followed by a further four hours at 75 °C in a thermostatted water bath. The resultant polydisperse zinc sulfide spheres were separated via centrifugation, rinsed and redispersed in argon-purged ethanol.

Resultant particle diameters varied from 0.5 to 20 μm, with the majority of particles possessing a diameter between 3 and 5 μm.

2.1.5. Cantilevers. Polycrystalline silicon cantilevers were fabricated using a standard lithography process (IMM, Mainz, Germany). The backside of cantilevers was then coated by sputtering gold before the spring constant was determined based on a resonance method [41]. The results were double checked against two reference cantilevers with careful manipulation such that only the ends of the cantilevers were in contact [33].

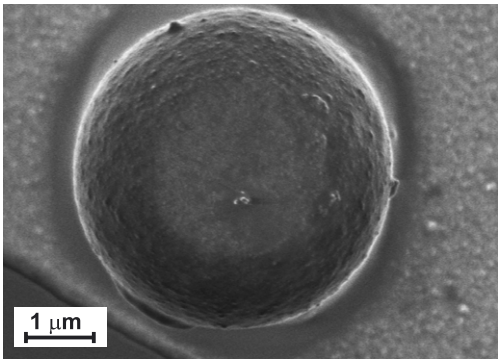

Figure 12. Scanning electron micrograph of a typical ZnS sphere, shown here attached to the apex of a cantilever. The length of the scale bar in the bottom left corner is 1 μm.

Sulfide mineral particles are known to oxidize in aerated water over time [42, 43] and thus expected to oxidize with exposure to air. To overcome this problem, zinc sulfide particles were attached (using a micromanipulator and Shell Epikote 1004) to cantilevers immediately prior to their use.

2.1.6. Determination of interaction forces. Particle–plate and particle–bubble interactions were determined using the PIA set-up described above. A special Teflon cuvette was built with only a small transparent quartz window to minimize the removal of zinc ions via adsorption from solution. All interactions were determined after a 3 h equilibration time. Particle–plate interactions were determined by pressing the colloid probe, either silica or zinc sulfide, against silica substrates, monitoring the deflection and piezo displacement. Particle–bubble interactions were determined in the same fashion after first aligning the particle approximately a few micrometres above the crest of the bubble with a micrometer screw driven by a stepper motors along X-, Y- and Z-axes. This was done under optical control of a microscope with a long-distance lens (magnification 120×), CCD camera and monitor. Loading (extend) and unloading (retract) force cycles were determined at 2.0 μm s^{-1} over trajectories of 12 μm in each direction. To quantify the force data the position sensitive device was calibrated from the constant compliance region of force curves. For particle–bubble interactions compliance slopes were determined against the solid substrate prior and subsequent to determining particle bubble interactions. The force (F) acting between the probe and bubble or surface was determined from the cantilevers deflection using Hooke's law, $F = k_c x$, where k_c represents the spring constant and x the deflection of the cantilever.

2.2. Results and discussion

2.2.1. ZnS–silica interaction. In all instances, the interactions between zinc sulfide particles and a silica substrate were found to be monotonically repulsive with decreasing separation. In previous studies of zinc sulfide, 'jump-in' features owing to van der Waals forces have only been seen at high electrolyte concentrations [44, 45] and not at concentrations used within the present study [44–47]. Atkins and Pashley [45] suggested that van der Waals forces were not resolvable owing to particle roughness, as is thought to be the case here. That is, SEM micrographs, for instance figure 12, show that ZnS particles possess a small but significant roughness. Interaction forces also show no short-range force associated with the hydration of

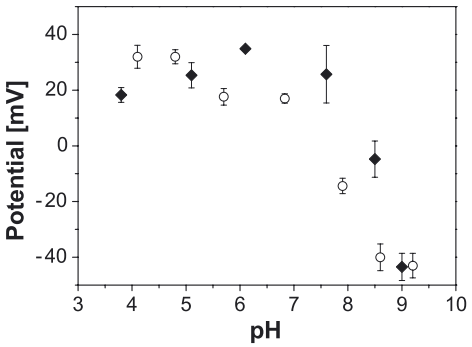

Figure 13. Comparison of surface potentials of zinc sulfide particles as a function of pH. Potentials were determined from the force between a silica substrate and zinc sulfide particles with radii between 1.5 and 3 μm in an electrolyte solution of 10^{-3} M KNO_3 10^{-4} M $Zn(NO_3)_2$ (♦) and 10^{-3} M KNO_3 10^{-5} M $Zn(NO_3)_2$ (○).

the silica surface, thus it follows that the interactions between silica and ZnS are governed by the overlap of electrical double layers.

The surface potential of ZnS particles was approximately determined by comparing force interactions between silica substrates and ZnS particles with a renormalized linear Poisson–Boltzmann equation. In doing this, the surface potential of the silica was first calculated from a silica probe–silica plate interaction, determined under identical conditions, so that only the surface potential of the ZnS was varied. Using the same approach, Toikka *et al* [47] reported the surface potential of ZnS particles in the absence of additional zinc ions, and concluded that the potentials were vastly different to those determined by techniques utilizing greater volumes fractions of ZnS particles. The reason for such a large discrepancy was suspected to be the zinc ion dissolution and the subsequent readsorption of hydrolysis species (see equations (3)–(5)) occurring to different extents in AFM experiments compared with techniques that require more concentrated dispersions.

$$\mathrm{ZnS} \rightarrow x\mathrm{Zn}^{2+}_{\mathrm{aq}} + \mathrm{Zn}_{(1-x)}\mathrm{S} \tag{3}$$

$$\mathrm{Zn}^{2+}_{\mathrm{aq}} + y\mathrm{OH}^{-} \rightarrow [\mathrm{Zn(OH)}^{2-y}_{y}]_{\mathrm{aq}} \tag{4}$$

$$[\mathrm{Zn(OH)}^{2-y}_{y}]_{\mathrm{aq}} \rightarrow [\mathrm{Zn(OH)}^{2-y}_{y}]_{\mathrm{ads}}. \tag{5}$$

For this reason, only the potentials of ZnS determined in solutions with additional zinc ions are presented. Surface potentials of zinc sulfide determined in 10^{-3} M KNO_3 in the presence of 10^{-4} and 10^{-5} M $Zn(NO_3)_2$, figure 13, suggest isoelectric points (IEPs) at approximately pH 8.5 and 7.5, respectively. The isoelectric point at pH 8.5 determined at 10^{-4} M Zn^{2+} is larger than expected for ZnS systems, and is likely to have resulted from the adsorption of excessive numbers of zinc ions. The isoelectric point of 7.5 determined at 10^{-5} M Zn^{2+} compares well with values reported by Ralston and co-workers [44, 46, 47] but disagrees with the IEP of 5.5 determined by Duran *et al* [48, 49]. The difference between these IEPs is considerable; for the purpose of this study we assume an IEP of pH 7.5 to represent the systems of interest, as Muster *et al* [46] have determined this value by both electrophoresis with a volume fraction of 2×10^{-4} and rheology studies with volume fractions of 0.1. Duran *et al* [48, 49] determined IEPs via laser Doppler velocimetry using a weight fraction of only 5×10^{-5}; it is plausible that at these slightly lower concentrations the surface potential becomes dependent on the volume fraction as observed in AFM studies [46, 47].

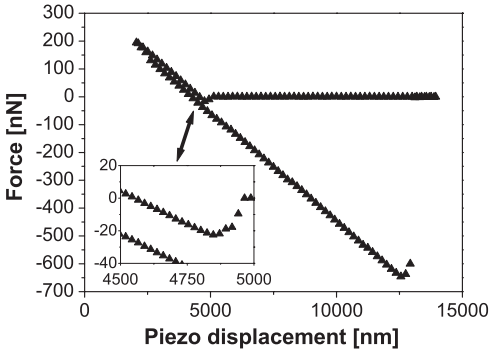

Figure 14. Force versus piezo displacement for a zinc sulfide particle interacting with a bubble determined in a solution of 10^{-3} M KNO_3 and 10^{-5} M $Zn(NO_3)_2$ at pH 7. For clarity only every third data point is displayed; the inset shows the region where the approach force becomes attractive due to particle bubble capillary forces. In this instance no initial repulsive force was observed and the point of contact was taken to be the last data point prior to attraction.

2.2.2. ZnS particle bubble interactions. A typical force versus piezo displacement for a ZnS particle interacting with a bubble is shown in figure 14. In general the adhesion showed no significant load dependence, which occurs when the immersion angle ω (figure 2, lower part) is less than the advancing contact angle [25]. Under these conditions, both the advancing and the receding contact angle can be calculated from force data.

Advancing contact angles were determined by fitting the adhesion to the maximum capillary force, whilst receding contact angles of ZnS particles were determined from force data using the analysis outlined above [33]. The use of the more sophisticated analysis [34] was not essential, as particles were larger than 5 μm. In this study the point of contact (in the absence of deformation and surface forces) was determined from an extrapolation of the linear region [23] prior to particle 'snap-in'. Such an approach is reported to be accurate within 25 nm [50].

For interactions determined in 10^{-3} M KNO_3, 10^{-5} M KNO_3 solution, contact angles of ZnS particles (figure 15) show a maximum of 95° and 74° for advancing and receding angles respectively at pH 7, with considerably smaller values under acidic and alkaline conditions. These experimental values correlate well with previously reported rheology data, overlaid in figure 15, and can be readily rationalized with respect to the surface electrical properties determined above. At pH values between 4–6 and 8–10, the surface chemistry is reasonably ionic owing to the presence of zinc, or zinc hydroxide species, the presence of which is likely to result in hydrophilic behaviour. At the IEP, the zero net charge means particles are less able to stabilize an aqueous film [51], resulting in significantly larger contact angles and more flocculation and thus a greater yield stress in more concentrated systems.

Force investigations of the zinc sulfide particles interacting with hydrophilic silica or a bubble in the presence of additional zinc ions suggest the IEP exists between pH 7 and 8. Such a finding correlates well with the ionic behaviour observed in techniques that require drastically larger volume fractions of zinc sulfide particles than in typical AFM studies.

3. The monolayer particle interaction apparatus (MPIA)

Force measurements with PIA in water containing charged detergents like SDS or DTAB revealed a delicate interplay of forces at the particle–water and the air–water interface.

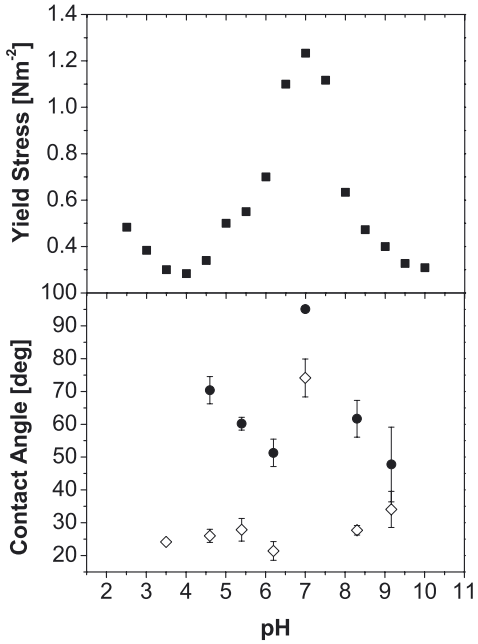

Figure 15. Advancing (●) and receding (◇) contact angles as a function of pH determined from the interaction forces between zinc sulfide particles with radii between 3 and 5 μm and a bubble (salt concentrations as in figure 14). The contact angles become maximal at a pH of 7, i.e. at the isoelectric point of the ZnS surface. A more hydrophobic behaviour of the ZnS particles at this pH will result in increased flocculation. This is reflected in the yield stress data (■) of ZnS slurries published by Muster *et al* [46], which are plotted on the secondary axis for comparison.

Depending on the detergent concentration, the surface energy of the colloidal particle, and the cantilever load, repulsion or adhesion between the two interfaces might be observed. While the qualitative interpretation of the force–distance curves is straightforward, a quantitative analysis of the molecular interaction turns out to be impossible because the exact amount of adsorbed detergent is unknown. In principle, the detergent might adsorb at the air–water and the particle–water interface due to different interactions. First, the adsorption at the air–water interface is favoured owing to the hydrophobic part of the detergent but counteracted by the intermolecular repulsion between their headgroups (figure 16(a)). Second, an adsorption to the solid particle is guided by the electrostatic or van der Waals interaction between detergent and solid surface. In the case of a hydrophobic particle, the interfacial energy of the particle–water interface is relatively high and adsorption of detergents via their alkyl chains is likely. This renders the particle surface more hydrophilic, thus decreasing its surface energy. Assuming simultaneous adsorption of the detergent to both interfaces, repulsion should be observable in any case because of the same sign of the charges within the detergent monolayer. In the case of a hydrophilic particle, the interfacial energy of the particle–water interface is low but detergents adsorb to oppositely charged solid particles. This renders the solid surface hydrophobic which is energetically unfavourable. Thus adsorption of an additional monolayer opposite to the first one (tail to tail) is very likely (figure 16(b)) [39]. In all scenarios hydrophobic or hydrophilic layers of alkyl chains or headgoups come into contact with water. Therefore, the force between the two discussed interfaces is mainly determined by the coverage of the amphiphilic detergents, as well as by its polarity and that of the particle.

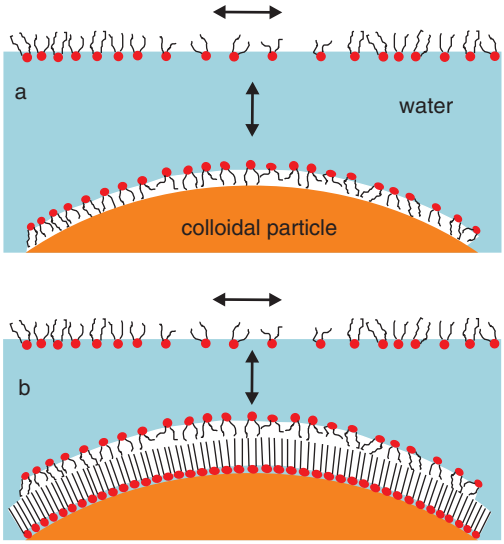

Figure 16. Scenarios of a colloidal probe approaching a monolayer of detergents. (a) A hydrophobic particle such as a polystyrene (PS) bead is likely to adsorb detergent from water to render the colloidal probe hydrophilic. (b) A hydrophilic particle such as a silicon bead adsorbs positively charged detergents from water, rendering the particle surface hydrophobic. An additional layer might be adsorbed for the surface to become hydrophilic again.

The effect of the different interactions on monolayer adhesion to planar silicon substrates has been studied in the Langmuir wetting configuration [52–54]. There, a silicon substrate was partially immersed into a water subphase in a Langmuir film balance [55]. A monolayer of an insoluble amphiphilic molecule is forming at the air–water interface after spreading, decreasing the surface energy of pure water ($\gamma_{lv} \approx 73$ mN m^{-1}) by orientation of alkyl chains to the air. The reduced surface tension is measured by the Wilhelmy plate method [56] and expressed as a quasi-two-dimensional pressure $\pi = \gamma_0 - \gamma_{lv}$. The molecular area is manipulated by movable barriers, by which the monolayer can be compressed (decreasing area) or expanded (increasing area). Isotherms, i.e. plots of the surface pressure versus the molecular area for measurements at constant temperature, reveal phase transitions within the swimming monolayer by kinks and plateaus. The insolubility of the amphiphiles ensures thereby that the monolayer is mechanically stable up to high surface pressures.

Figure 17 shows the isotherm of the frequently used lipid dimyristoylphospatidyl-ethanolamine, DMPE. At large molecular areas the monolayer is in a disordered liquid-expanded (LE) phase whereas at low molecular areas in the liquid-condensed (LC) phase it shows ordering mainly due to the orientation of alkyl chains [57]. In the plateau the monolayer shows a phase transition from LE to LC phase. DMPE is a dipolar molecule and an electrostatic attraction between its headgroups and the negatively charged silicon surface can be expected. Visualized by fluorescence microscopy [58], this attraction leads to a condensation of the expanded monolayer on the water (bright) into a LC phase on the substrate (dark) at the three-phase contact line between silicon, air and water [53]. This condensation has been quantified by very accurate contact angle measurements [54] as the work of adhesion for the monolayer-wetted silicon substrate. The condensation occurs in a range of about 3 mN m^{-1} within the LE phase only, revealing again a delicate interplay of different molecular interactions between substrate and monolayer.

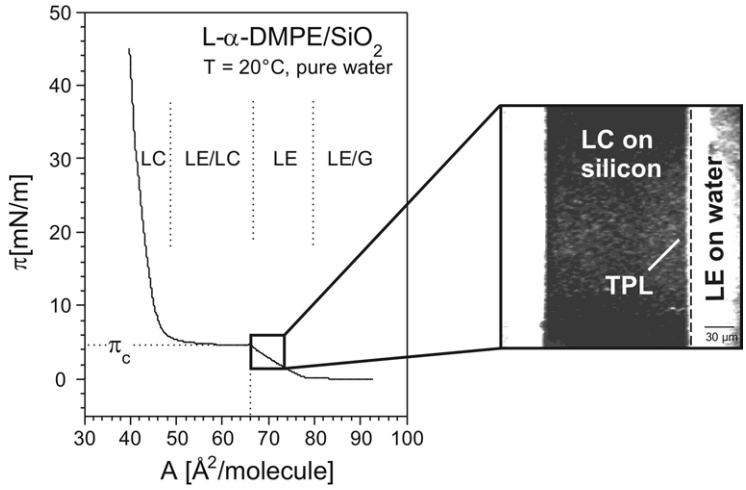

Figure 17. Isotherm of a monolayer of dimyristoylphosphatidylethanolamine (DMPE), a well studied insoluble lipid. The plateau at about 5 mN m^{-1} indicates a phase transition from an isotropic liquid-expanded (LE) to an ordered liquid-condensed (LC) phase. Before the phase transition at the air–water interface an immersed negatively charged silicon substrate induces a phase transition in the ultra-thin film during transfer from water to silicon surface. This can be seen as a dye-depleted stripe on the substrate by fluorescence microscopy.

To better understand the role of these interactions a set-up is desired which allows measurement of force–distance curves at well defined molecular areas of the monolayer as well as contact angles. For this we integrated the colloidal probe technique into a Langmuir film balance (figure 18). The combination of the two methods ensures that molecular interactions can be quantified as well as that the colloidal probe is wetted in a definite way. Adsorption at the colloidal particle surface, which approaches from below to the monolayer, can be neglected before the first particle–monolayer contact. Monolayer desorption from the particle can be achieved by a short waiting time after a small retraction step from the film–water interface.

The new instrument consists of a custom film balance (R&K Ultrathin Organic Film Tech., Germany), a particle interaction apparatus (PIA) and a fluorescence microscope (Axiotech Vario, Carl Zeiss, Germany). The barriers of the Langmuir trough can be decoupled, thus allowing usual compression/expansion cycles and alternatively the investigation of different surface areas by parallel movement of the barriers. Different phases within one monolayer are visualized by fluorescence microscopy such that the objective and the colloidal probe are aligned. The temperature in the film balance is kept constant with a water thermostat (Phönix P1-C25P, Thermo Haake, Germany). To prevent vibrations the film balance and PIA are positioned on an active vibration table (TS140, HWL Scientific Instruments, Germany).

PIA is integrated into the film balance through a quartz glass window inside a Teflon pot in the middle of the balance. It can be removed by screwing for better cleaning. The cantilever holder made of polyaryletheretherketone (PEEK) can be edged through a PEEK bearing in the glass window, sealed by silicone fittings. The holder is arranged on one platform together with a laser light source ($\lambda = 660 \pm 5$ nm, $P = 5$ mW, Hofmann and Schäffter, Germany) and a two-dimensional photosensitive diode (Laser Components, Germany). In this set-up, the laser beam is directed upwards through the glass window and reflected from the outmost rim of the cantilever into the water subphase. After passing the window again it is reflected from a mirror onto the position sensitive detector (PSD). The cantilever can be moved perpendicular to the water surface with a translation stage (HVM60, Owis, Germany) for first surface approach

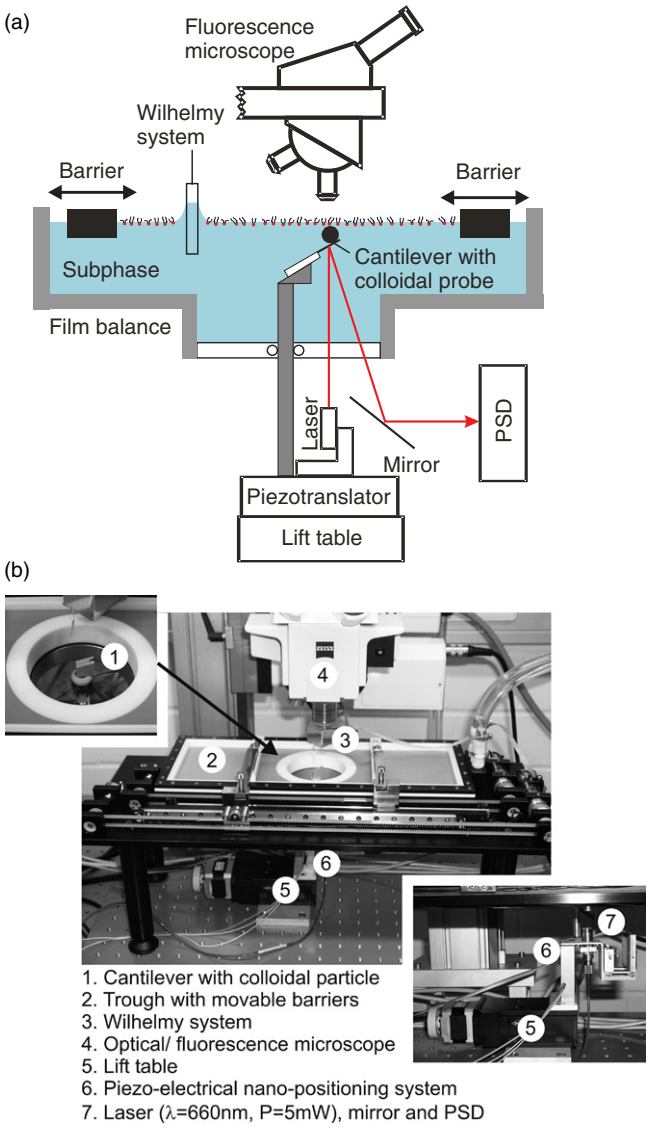

Figure 18. Set-up of the monolayer particle interaction apparatus (MPIA). Schematic (a) and photo (b) of MPIA (for explanations, see text).

and with a piezo-electrical nano-positioning system (LISA, Physik-Instrumente, Germany) for measurement with a distance resolution of <1 nm using a capacitive sensor within a range of 25 μm. The laser can be adjusted to the cantilever by screws. The mirror below the quartz window enables us to direct the reflected laser beam onto the centre of the PSD. The laser deflection is measured as PSD voltage (± 10 V) with a resolution of 16 bits.

4. Summary

The colloidal probe technique is a valuable method to measure forces between solid particles as made from silicon, polymer or insoluble salt crystals and the air–water interface. The

repulsion between charged surfaces and the adhesion of non-charged particles to the water surface is greatly influenced by the presence of detergent in the water. Depending on the charge of the solid particle and the detergents as well as their concentration, repulsion and adhesion can be changed. This effect also depends on the load of the cantilever applied, revealing adsorption/desorption of detergent molecules from both the air–water and particle–water interfaces. For better understanding of the interactions on a molecular level a modified particle interaction apparatus has been constructed by combining it with a Langmuir film balance. This allows maintenance of a definite surface density of amphiphilic molecules at the air–water interface. This new instrument offers the possibility to investigate the role of molecular interactions for wetting of microscopic particles.

Force investigations of zinc sulfide particles interacting with hydrophilic silica or a bubble in the presence of additional zinc ions suggest the IEP exists between pH 7 and 8. Such a finding correlates well with the ionic behaviour observed in techniques that require drastically larger volume fractions of such particles than in typical AFM studies.

Acknowledgment

We thank the Deutsche Forschungsgemeinschaft for financial support.

References

[1] Bartell F E and Osterhof H J 1927 *Z. Phys. Chem.* **130** 715
[2] Bartell F E and Jennings H Y 1934 *J. Phys. Chem.* **38** 495
[3] Bruil H G and van Aartsen J 1974 *Colloid Polym. Sci.* **252** 32–8
[4] Siebold A, Walliser A, Nardin M, Oppliger M and Schultz J 1997 *J. Colloid Interface Sci.* **186** 60–70
[5] Grundke K, Bogumil T, Gietzelt T, Jacobasch H J and Neumann A W 1996 *Prog. Colloid Polym. Sci.* **101** 58–68
[6] Lucas R 1918 *Kolloidn. Zh.* **23** 15–22
[7] Washburn E W 1921 *Phys. Rev.* **17** 273–83
[8] Levine S, Lowndes J, Watson E J and Neale G 1980 *J. Colloid Interface Sci.* **73** 136–51
[9] Van Brakel J 1975 *Powder Technol.* **11** 205–36
[10] Leja J 1982 *Surface Chemistry of Froth Flotation* (New York: Plenum)
[11] Schulze H J 1984 *Physico-Chemical Elementary Prosesses in Flotation* (Amsterdam: Elsevier)
[12] Janczuk B 1983 *J. Colloid Interface Sci.* **93** 411–8
[13] Clint J H and Taylor S E 1992 *Colloids Surf.* **65** 61–7
[14] Clint J H and Quirke N 1993 *Colloids Surf.* A **78** 277–8
[15] Yarnold G D 1946 *Proc. Phys. Soc.* **58** 120–5
[16] Scheludko A D and Nikolov A D 1975 *Colloid Polym. Sci.* **253** 396–403
[17] Huh C and Mason S G 1976 *Can. J. Chem.* **54** 969–78
[18] Bayramli E, Huh C and Mason S G 1978 *Can. J. Chem.* **56** 818–23
[19] Bayramli E and Mason S G 1982 *Colloid Polym. Sci.* **260** 452–3
[20] Gunde R, Hartland S and Mäder R 1995 *J. Colloid Interface Sci.* **176** 17–30
[21] Zhang L, Ren L and Hartland S 1996 *J. Colloid Interface Sci.* **180** 493–503
[22] Zhang L, Ren L and Hartland S 1997 *J. Colloid Interface Sci.* **192** 306–18
[23] Ducker W A, Xu Z and Israelachvili J N 1994 *Langmuir* **10** 3279–89
[24] Butt H-J 1994 *J. Colloid Interface Sci.* **166** 109–17
[25] Fielden M L, Hayes R A and Ralston J 1996 *Langmuir* **12** 3721–7
[26] Preuss M and Butt H-J 1998 *Langmuir* **14** 3164–74
[27] Scheludko A, Toshev B V and Bojadjiev D T 1976 *J. Chem. Soc. Faraday Trans.* I **72** 2815–28
[28] Ralston J and Newcombe G 1992 *Colloid Chemistry in Mineral Processing* ed J S Laskowski and J Ralston (Amsterdam: Elsevier)
[29] Butt H-J, Ecke S, Heim L O, Heiskanen K, Preuss M, Raiteri R, Schreithofer N, Vinogradova O I and Yakubov G E 2002 *Contact Angle, Wettability and Adhesion* vol 2, ed K L Mittal (Zeist: VSP)
[30] Dubois L H and Nuzzo R G 1992 *Annu. Rev. Phys. Chem.* **43** 437–63
[31] Xu J and Li H-L 1995 *J. Colloid Interface Sci.* **176** 138–49

[32] Ulman A 1996 *Chem. Rev.* **96** 1533–54
[33] Preuss M and Butt H-J 1998 *J. Colloid Interface Sci.* **208** 468–77
[34] Yakubov G E, Vinogradova O I and Butt H-J 2000 *J. Adhes. Sci. Technol.* **14** 1783–99
[35] *Beilstein (BRN 3599286 for SDS.; BRN 3597463 for DTAB)*
[36] Yoon R H, Flinn D H and Rabinovich Y I 1997 *J. Colloid Interface Sci.* **185** 363–70
[37] Dai Q, Sasaki H, Usui S and Kaisheva M 1990 *J. Colloid Interface Sci.* **139** 30–42
[38] Eriksson J C and Ljunggren S 1995 *Langmuir* **11** 2325–8
[39] Eriksson L G T, Claesson P M, Eriksson J C and Yaminsky V V 1996 *J. Colloid Interface Sci.* **181** 476–89
[40] Wilhelmy D M and Matijevic E 1984 *J. Chem. Soc., Faraday Trans.* I **80** 563–70
[41] Sader J E, Chou J W M and Mulvaney P 1999 *Rev. Sci. Instrum.* **70** 3967–9
[42] Fornasiero D, Li F S and Ralston J 1994 *J. Colloid Interface Sci.* **164** 345–54
[43] Simpson S L, Apte S C and Batley G E 1998 *Environ. Sci. Technol.* **32** 620–5
[44] Toikka G, Hayes R A and Ralston J 1996 *Langmuir* **12** 3783–8
[45] Atkins D T and Pashley R M 1993 *Langmuir* **9** 2232–6
[46] Muster T H, Toikka G, Hayes R A, Prestidge C A and Ralston J 1996 *Colloids Surf.* A **106** 203–11
[47] Toikka G, Hayes R A and Ralston J 1998 *Colloids Surf.* A **141** 3–8
[48] Duran J D G, Ontiveros A and Chibowski E 1999 *J. Colloid Interface Sci.* **214** 53–63
[49] Duran J D G, Guindo M C and Delgado A V 1995 *J. Colloid Interface Sci.* **173** 436–42
[50] Dagastine R R, Prieve D C and White L R 2004 *J. Colloid Interface Sci.* **269** 84–96
[51] Blake T D and Kitchener J A 1972 *J. Chem. Soc., Faraday Trans.* I **68** 1435–42
[52] Petrov J G, Kuhn H and Möbius D 1980 *J. Colloid Interface Sci.* **73** 66–75
[53] Riegler H and Spratte K 1992 *Thin Solid Films* **210** 9–12
[54] Graf K and Riegler H 1998 *Colloids Surf.* A **131** 215–24
[55] Langmuir I 1920 *Trans. Faraday Soc.* **15** 62–74
[56] Wilhelmy L 1863 *Ann. Phys. Chem.* **119** 177–217
[57] Helm C A, Tippmann-Krayer P, Möhwald H, Als-Nielsen J and Kjaer K 1991 *Biophys. J.* **60** 1457–76
Möhwald H, Böhm C, Dietrich A and Kirstein S 1993 *Liq. Cryst.* **14** 265–77
[58] Lösche M, Sackmann E and Möhwald H 1983 *Ber. Bunsenges. Phys. Chem.* **87** 848–52
[59] Ecke S, Preuss M and Butt H-J 1999 *J. Adhes. Sci. Technol.* **13** 1181–91